WILEY The International Journal of **Medical Robotics** and **Computer Assisted Surgery**

ORIGINAL ARTICLE

Real-time simulation of soft tissue deformation and electrocautery procedures in laparoscopic rectal cancer radical surgery

Yuan Sui[1] | Jun J. Pan[1] (ORCID) | Hong Qin[2] | Hao Liu[3] | Yun Lu[4]

[1] State Key Laboratory of Virtual Reality Technology and Systems, Beihang University, Beijing, China

[2] Department of Computer Science, Stony Brook University (SUNY Stony Brook), Stony Brook, New York, USA

[3] State Key Laboratory of Robotics, Shenyang Institute of Automation, Chinese Academy of Sciences, Shenyang, China

[4] The Affiliated Hospital of Qingdao University, Qingdao, China

Correspondence
Jun J. Pan, State Key Laboratory of Virtual Reality Technology and Systems, Beihang University, Beijing, China.
Email: pan_junjun@hotmail.com

Abstract

Background: Laparoscopic surgery (LS), also referred to as minimally invasive surgery, is a modern surgical technique which is widely applied. The fulcrum effect makes LS a non-intuitive motor skill with a steep learning curve.

Methods: A hybrid model of tetrahedrons and a multi-layer triangular mesh are constructed to simulate the deformable behavior of the rectum and surrounding tissues in the Position-Based Dynamics (PBD) framework. A heat-conduction based electric-burn technique is employed to simulate the electrocautery procedure.

Results: The simulator has been applied for laparoscopic rectum cancer surgery training. From the experimental results, trainees can operate in real time with high degrees of stability and fidelity. A preliminary study was performed to evaluate the realism and usefulness.

Conclusions: This prototype simulator has been tested and verified by colorectal surgeons through a pilot study. They believed both the visual and the haptic performance of the simulation are realistic and helpful to enhance laparoscopic skills.

KEYWORDS

dissection simulation, laparoscopic rectal surgery, position-based dynamics, soft tissue deformation

1 | INTRODUCTION

Laparoscopic surgery (LS) is one of modern minimally invasive surgery (MIS) techniques, which adopts small incisions and long pencil-like instruments to perform operations with a camera. In recent years, when performing surgery, MIS has become increasingly popular due to its smaller scars and less pain. Compared with conventional open surgery, patients who choose laparoscopic surgery usually have shorter hospital stays, quicker recovery, and less post-operative complications.[1] Procedures such as hernia repairs, gastric bypass, bowel resection, and organ removal are now routinely carried out laparoscopically. Colon and rectum cancer is the fourth most common cancer, and represents 8% of all new cancer cases in America. In 2016, it was estimated that there would be 134 490 new cases of colon and rectum cancer and an estimated 49 190 people would die of this disease.[2] Laparoscopic surgery for rectal cancer (Figure 1,[3] and Figure 2) is a safe and established alternative to traditional open rectectomy.[4] The last 5 years have seen a significant advancement of laparoscopy for colorectal cancer which has resulted in evolvement of new techniques and their integration into current practice.

Due to the different hand–eye coordination, lacking a sense of depth on the 2D video stream captured by the laparoscope, and the fulcrum effect of long instrument manipulation, LS is generally difficult to learn by conventional apprenticeship practice through observation and imitation. Basic LS technical skills such as suturing and ligation could be trained by laparoscopic box.[5] However, due to the lack of realistic visual and tactile feeling of human tissues, novice surgeons and residents usually choose training by directly performing the surgery on real patients under the supervision of senior surgeons.

A virtual-reality (VR) based simulator, which offers a safe, efficient, repetitive and low cost solution, has been developed to overcome the above difficulties in training. There are already several commercial VR based LP simulators: LapSim (http://www.surgical-science.com/), Lap Mentor (http://simbionix.com/simulators/) etc. in the market. They provide training functions in cholecystectomy (gallbladder removal),
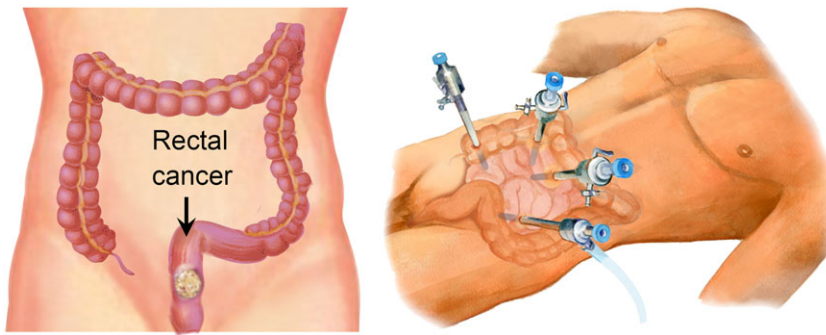
FIGURE 1 Location of rectal cancer (*left*) and the placement of laparoscope, grasper and electrosurgical scalpel in abdominal cavity for laparoscopic rectal cancer radical surgery (*right* (3))

FIGURE 2 Real operation environment for laparoscopic rectal cancer radical surgery

ectopic pregnancy, myomectomy and so on. At present, colorectal cancer is the fifth commonest cancer in China, with one new case diagnosed every 1.5 min on average,[6] and 90% of cases are suitable for laparoscopic surgery. However, in hospitals there is a relative lack of surgeons trained to perform such complex surgery. This is particularly true for rectal cancer radical surgery, which is the most technically challenging for the laparoscopic colorectal surgeon. Therefore, we decided to focus on rectal cancer radical surgery simulation.

Many existing simulation systems use a mass–spring system (MSS) as the physical model of soft tissue due to its simplicity.[7-9] A vital drawback of the MSS method is that it cannot reflect volumetric effects, such as volume conservation or the prevention of volume inversions,[10] which limits the physical accuracy. Another popular approach is the finite element method (FEM),[11] which treats the deformable tissue as a continuous volume and solves the problem by continuum mechanics.[12] Although FEM can fix volumetric problems of MSS, it is too time-consuming to perform real-time simulation in some complex surgery scenes.

Electrosurgery, which indicates the application of high-frequency electric current to dissect human tissue by heat, is an essential procedure for most laparoscopic surgeries. Physics-based electrosurgical

cautery simulation is an important research topic in VR laparoscopic simulator. Dodde et al.[13] analysed temperature distribution in biological tissue subject to a bipolar electrosurgical procedure under the FEM framework. Maciel et al.[14] implemented a physics-based model of electrosurgery to control the temperature distribution in tissue as a function of time. Lu et al.[15] demonstrated a physics-based electrosurgery cutting algorithm and designed a topology change with low computational cost in 2014. Wu et al.[16] presented a highly efficient and physically accurate real-time cutting simulation method. They proposed the semi-regular hexahedral finite element grid as the basic element in their physical system. Qian et al.[17] proposed an energized soft tissue dissection model. They classify the soft tissues into three types (fascia, membrane, and fat) and simulate their physical properties accordingly under the projective dynamics framework. An edge-based structure for the dissection algorithm is proposed, which offers an effective mechanism simulation, while not changing the mesh topology.

This paper aims to describe the technical details of our simulator for laparoscopic rectal cancer radical surgery. The innovative contributions consist of the design of laparoscopic instrument handle, deformation of rectum by multi-layer PBD model, simulation of electrocautery

on membrane tissues. We demonstrated the experimental results of our simulator in visual performance and computational cost at the stage of soft tissue deformation, and compared it with results from the prototyped system of Pan et al.[18] A pilot study by questionnaire for surgeons was also used to prove the validation and realism of the simulator.

2 | MATERIALS AND METHODS

As shown in Figure 3, the hardware of our simulator consists of a LED monitor, a wireless keyboard, a foot pedal, a workstation with two haptic devices inside the simulator, and two laparoscopic instrument handles outside. We use Geomagic Touch (Phantom Omni of Sensible) as haptic feedback device, which could offer 6DOF input data with a resolution of 0.009 mm in 3D space, and up to 3.3 N 3DOF force output.[19] Although the Phantom Omni cannot provide the moment of force, we choose it as haptic device due to its continuous and stable performance in force output. In addition, its advantages of low cost and small size are suitable for it to be installed in our prototyped simulator. We modified the surgery instrument handle to get the

FIGURE 3 Hardware interface of our simulator, including (from top to bottom) touch screen, keyboard, simulator case with surgery handles, and foot pedal

continuous angle between two jaws of a grasper. Figure 4 is a snapshot of the software interface for our simulator. It illustrates the anatomy of a segment of rectum, membrane tissue, retroperitoneum and abdominal wall. The software is developed with OpenGL, Openhaptics and C++. Based on the MRI data, we build 3D models of human organs which fit the characteristics of the Chinese, under the guidance of colorectal surgeons from The Affiliated Hospital of Qingdao University. To improve the realism of anatomy and interaction, we add two layers of semi-transparent membrane tissue meshes covering the rectum.

The simulation consists of an off-line stage and online stage. In the off-line stage, a tetrahedral rectum model with stretch, bending and volume constraints is constructed initially. Next, springs linked between the tetrahedral rectum model and the triangular mesh of the membrane tissue are connected. In the online stage, the system collects input data from the haptic devices, detects collisions, computes deformation and temperature distribution, updates textures and topologies, and renders them graphically and haptically. Figure 5 illustrates the software architecture of our system. Technically, there are three innovative contributions:

1. a customized laparoscopic instrument handle offering continuous variable angle between two jaws of a grasper or scissors;

2. a multi-layer mechanical model to handle the soft tissue deformation of rectum, under the PBD framework;

3. bio-heat conduction based electrocautery simulation, which supports real-time topological change and realistic graphic rendering, designed for membrane tissue dissection.

3 | MODIFICATION OF SURGICAL INSTRUMENT HANDLE

In laparoscopic surgery, surgeons hold the handle and rotate it to control the angle between two jaws of a grasper or scissors. In simulator hardware design, how to collect the digital value of this jaw angle is a technical challenge. Here, as illustrated in Figure 6, we modify the mechanical structure of the laparoscopic surgery handle to add electronic components, which can collect the digital value of the variable angle between the two jaws smoothly. At the beginning, we plan to use a slide rheostat to detect the rotation angle of the handle arms,
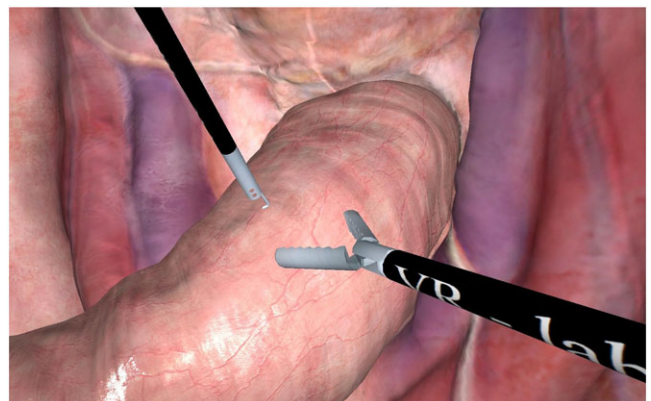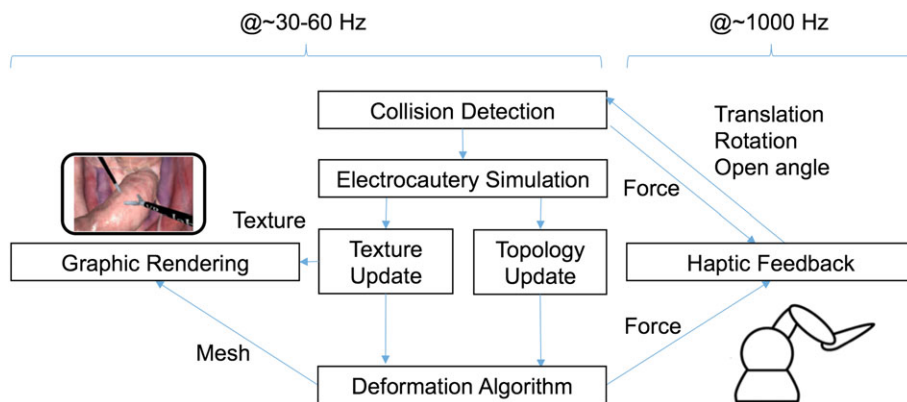

FIGURE 4 Software interface of our simulator

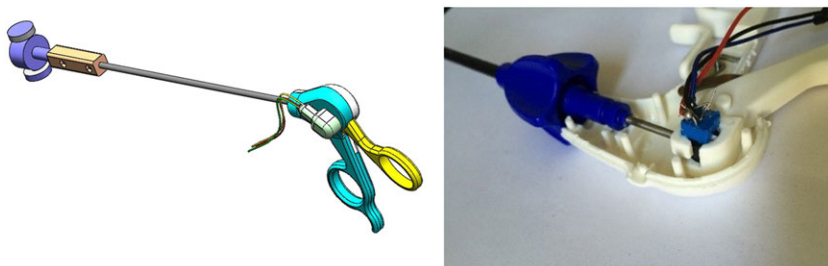**FIGURE 5** Software architecture of simulation system

FIGURE 6 Design of simulator handle (*left*) and internal structure of modified surgery handle (*right*)

however, due to the mechanical friction, there is an evident resistance when rotating the handle arms. Finally, we chose the mini potentiometer to detect the angle.

We fix the potentiometer on the axis of the handle, and connect the potentiometer axis to the handle. So when a voltage is supplied to the potentiometer, we obtain different voltage values according to the angle between the two arms. Then we use PIC24FJ64GA002 (Figure 7). which contains an A/D chip, to convert the analog signal to a digital signal. In the setting of A/D module, we use timer 3 in PIC24 to control the sampling time and set it to 2.5 ms per sample, waiting for the delay of signal processing. The A/D conversion gives us an integer ranging from 0 to 1024, which means it has a resolution of 2^{10}, and we multiply this integer by 0.00488 V ($5V/2^{10}$) for normalization.

Finally, we transmit the digital data to our system by a UART in PIC24 and a serial-to-TTL cable. Since the UART translates bits of the voltage value into characters, we use the serial mode and set the baud rate as 115200 to read and parse the received characters. Figure 6 shows the sensor and the A/D converter of the modified surgery handle. The final digital output is in the range from 2.37 V to 2.54 V, with an error ±0.002V. And this digital voltage value is converted to the jaws angle from 0 degree to 60 degree in the system.

4 | DEFORMATION OF SOFT TISSUE

For colorectal surgery simulation, due to the frequent large movement and deformation of the intestine during operation, it is a great challenge to compute the deformation of soft tissues realistically in real time. The complex biological environment around the rectum, consisting of the membrane and fat tissue, brings more difficulties in simulation of their mechanical behavior.

Many approaches have been adopted in graphics, such as the Finite Element Method (FEM), the Mass-Spring System (MSS), and Position-Based Dynamics (PBD). MSS is one of the simplest approaches to simulate deformable objects by establishing springs between particles.[20] Because of its simplicity, it is an ideal framework for many interactive applications. However, MSS cannot reflect volumetric effects, such as volume conservation or the prevention of volume inversions.[10] Finite element method FEM subdivides a model into finite smaller and simpler elements and obtains results by solving partial differential equations.[21] Although FEM has been widely used in the fields of industry, film, and architecture for its physical accuracy, limited by its complex computation, FEM may not be a suitable solution for our application in real time. While some real-time simulations of relatively simple models can be achieved using the FEM
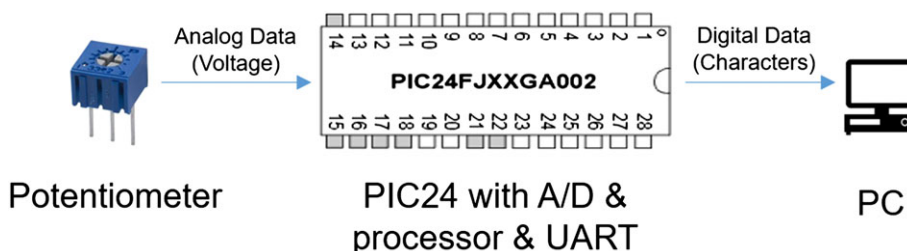

FIGURE 7 PIC24 and its work flow

method,[22,23] the computational cost is heavy, especially for large movement and deformation frequently taking place in the intestine during laparoscopic rectal cancer radical surgery. In addition, when cutting occurs in FEM, it is necessary to update the global matrix at every time step in dealing with the topology change. This process is usually too time-consuming to run in real time for relatively complex models.

For this simulation, speed and controllability are the primary factors to be considered. As a secondary factor, we want physical computation as accurate as possible. A position-based method provides a high level of interaction controllability and stable performance even when simple and fast explicit time integration schemes are used.[24,25] An extended PBD that accommodates the topology modification has been shown to be capable of handling soft tissue deformation and dissection.[26] This approach is a compromise between FEM and MSS in aspects of both efficiency and accuracy. For the above reasons, we prefer to construct a multi-layer PBD model in our application scenario.

Under the framework of PBD, different types of physics-based constraints can be customized and handled specially for our surgery scene. Therefore, it is particularly well suited to our specific surgery scene with complex biological environment. In the off-line stage of our program, we construct customized constraints for both the rectum model and the membrane tissue model. Then these separate models are integrated into a whole physical system using springs.

To describe the volume conservation of the rectum, we subdivided the rectum model into many small tetrahedrons. For each one of them, we initialize its four vertexes with positions, velocities and mass as initial physical status. Two types of internal constraints are given to provide a restoring force:

(1) **Stretch constraints**. We establish stretch constraints along the edges of tetrahedrons (Figure 8) to restrict the distance between two vertexes. It can be described as:

$$C_{stretch}(\mathbf{p}_1, \mathbf{p}_2) = |\mathbf{p}_1 - \mathbf{p}_2| - d \qquad (1)$$

where d is the rest length of the edge. m_1 and m_2 indicate the mass of particle $\mathbf{p}_1$ and $\mathbf{p}_2$. The final positional corrections of the stretch constraint are given in the Appendix A1.

(2) **Volume conservation constraints**. We give every single tetrahedron a volume conservation constraint (Figure 9). which defines the particles ($\mathbf{p}_1, \mathbf{p}_2, \mathbf{p}_3, \mathbf{p}_4$) at the corners of the tetrahedron. It is designed to maintain the initial volume of each tetrahedron and then maintain the total volume. The volume conservation constraint can be described as:
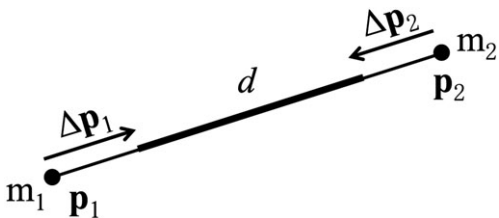

FIGURE 8 Illustration of stretch constraint between $\mathbf{p}_1$ and $\mathbf{p}_2$ for an edge
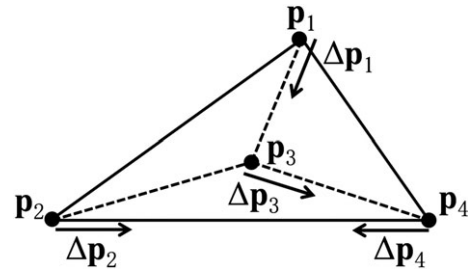

FIGURE 9 Illustration of volume conservation constraint

$$C_{volume}(\mathbf{p}_1, \mathbf{p}_2, \mathbf{p}_3, \mathbf{p}_4) = \frac{1}{6}((\mathbf{p}_2 - \mathbf{p}_1) \times (\mathbf{p}_3 - \mathbf{p}_1)) \cdot (\mathbf{p}_4 - \mathbf{p}_1) - V_0 \qquad (2)$$

where V_0 is the initial volume of tetrahedron. The final positional corrections of the volume constraint are given in the Appendix A2.

To simulate the behavior of the membrane tissue surrounding the rectum, we add a triangular surface mesh and construct a physical model for it. Similarly, we initialize the physical status for each vertex and define two different types of internal constraints: (1) stretch constraints, and (3) **Bending constraints**. Here, resistances derived from bending constraints conserve the dihedral angle between two adjacent triangles. While moving, the projection point for each particle is updated accordingly and the bind constraint push or pull the particle to maintain the rest distance. The bending constraint can be described as:

$$C_{bending}(\mathbf{p}_1, \mathbf{p}_2, \mathbf{p}_3, \mathbf{p}_4) = arc\cos\left(\frac{(\mathbf{p}_2 - \mathbf{p}_1) \times (\mathbf{p}_3 - \mathbf{p}_1)}{|(\mathbf{p}_2 - \mathbf{p}_1) \times (\mathbf{p}_3 - \mathbf{p}_1)|} \cdot \frac{(\mathbf{p}_2 - \mathbf{p}_1) \times (\mathbf{p}_4 - \mathbf{p}_1)}{|(\mathbf{p}_2 - \mathbf{p}_1) \times (\mathbf{p}_4 - \mathbf{p}_1)|}\right) - \varphi_0 \qquad (3)$$

where φ_0 is the initial dihedral angle. The final positional corrections of the bending constraint are given in the Appendix A3. The following paragraphs give a brief introduction to the mathematical foundations of the PBD method.[27]

Given the vector of vertexes position $\mathbf{x} = (x_1, x_2, \cdots x_n)^T$ and velocity $\mathbf{v} = (v_1, v_2, \cdots v_n)^T$, the system employs a simple Euler integration to predict positions and velocities at the next time step. The system solves a nonlinear system of equalities and inequalities to satisfy the following internal constraints:

$$C_i(\mathbf{x} + \Delta\mathbf{x}) \succ 0, i = 1, 2, \cdots m, \qquad (4)$$

where the symbol $\succ$ denotes either = or ≥, m is the number of constraints. Using a non-linear Gauss–Seidel method, each constraint equation is linearized to

$$C_i(\mathbf{x}) + \nabla C_i(\mathbf{x}) \cdot \Delta\mathbf{x} \succ 0, i = 1, 2, \cdots m, \qquad (5)$$

and can be solved separately by restricting $\Delta\mathbf{x}$ to be in the direction of ∇C. The correction vector of single vertex is calculated with the following form:

$$\Delta\mathbf{x}_i = -\lambda_i \omega_i \nabla_{\mathbf{x}_i} C(\mathbf{x}), \qquad (6)$$

where $\omega_i = 1/m_i$ and λ_i is a Lagrange multiplier

$$\lambda_i = \frac{C_i(\mathbf{x})}{\sum_i \omega_i |\nabla_{\mathbf{x}_i} C(\mathbf{x})|^2}. \qquad (7)$$

After several iterations, the correction of positions $\Delta\mathbf{x}_i$ can be used to update the positions and velocities. Since the final deformation

behavior results from several factors, such as length of time step, iteration times and stiffness of different constraints, it is hard to adjust these parameters to ideal values at one time.

5 | MULTI-LAYER PBD MODEL

To better describe the mechanical behaviour of the fat tissues between the rectum and membrane, we create a multi-layer structured PBD model, consisting of a dynamic layer and an interpolative layer. The dynamic layer has its own mass nodes as physical model, which can be generated by uniform re-sampling from the original surface mesh model of the membrane. The interpolative layer does not participate in physical computation. The role of the interpolative layer is to visually simulate the thick layer of fat when interactions occur between surgery tools and the dynamic layer. Figure 10 shows the relationship between: rectum, membrane, tetrahedral mesh, surface mesh, dynamic layer, and interpolation layer. The dynamic layer is a surface mesh of the membrane. The tetrahedral mesh is the physical model of the rectum. Both the dynamic layer and the tetrahedral mesh together make up the PBD simulation system, while the interpolative layer ONLY participates in visual rendering. The interpolative layer can be updated by the dynamic layer and tetrahedral mesh at the end of each time step. The simulation of electrocautery only affects the dynamic layer by updating its texture and topology.

In the off-line stage, the dynamic layer is constructed from the original mesh model. As we have a high-resolution mesh with uniform triangular distribution, we sort these mass nodes by their positions to set up constraints in an intuitive way. Another advantage of rearranging the mass nodes by rows and columns is the maintainability and extensibility. We can efficiently manipulate the constraints when topological changes occur, and down-sample the physical nodes regularly if necessary. For each vertex p_i, we add three stretch constraints to its neighbouring vertices. Figure 11 illustrates this process and the connected stretch constraints are: $C_{stretch}(p_{i,j}, p_{i+1,j})$, $C_{stretch}(p_{i,j}, p_{i,j+1})$ and $C_{stretch}(p_{i,j}, p_{i+1,j+1})$. As mentioned earlier, bilateral bending constraints are constructed for the shared edges of adjacent triangles. We obtain the following equation:
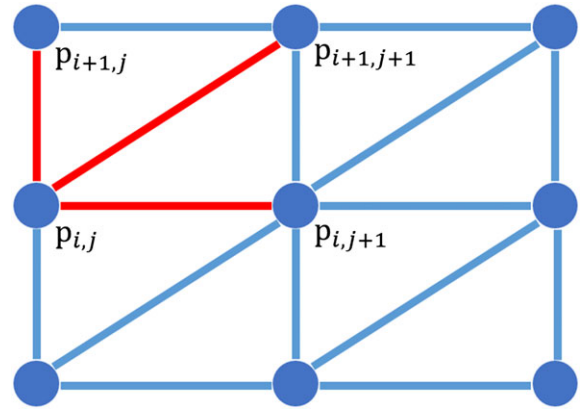

FIGURE 11 Construction of stretch constraints on the membrane mesh

$$C(\mathbf{x}_1, \mathbf{x}_2, \mathbf{x}_3, \mathbf{x}_4) = \arccos(\mathbf{n}_1 \cdot \mathbf{n}_2) - \varphi_0, \qquad (8)$$

where φ_0 is the initial dihedral angle between adjacent triangles on different sides; $\mathbf{n}_1$, $\mathbf{n}_2$ are normal vectors of adjacent triangles. To avoid exaggerated deformation, nodes located at both the far-end and near-end of the membrane model are fixed. Finally, as shown in Figure 12, each mass node on the dynamic layer of the membrane searches a linked vertex on the surface of the rectum, according to the following object function:

$$\min_p \|\mathbf{x}_p - \mathbf{x}_q\| - \mathbf{n}_p \cdot \mathbf{n}_q + \delta(\|\mathbf{x}_p - \mathbf{x}_q\|), \qquad (9)$$

where $\mathbf{n}_p$ is the normal vector of the vertex on the dynamic layer with index p; $\mathbf{n}_q$ is the normal vector of the vertex on the surface of the rectum with index q; δ is an indicator function, whose value turns out to be infinite when the Euclidean distance of $\mathbf{x}_p$ and $\mathbf{x}_q$ exceeds a threshold, otherwise it is zero. These global springs bind the dynamic layer of the membrane and the tetrahedral model of the rectum together as an integrated physical system. To maintain real-time computation efficiency, we do not connect the rectum with other organs in the physical system. But we construct a simple PBD surface model for the retroperitoneum and abdominal wall, to help the user identify the ureter and interact in a relatively completed abdominal environment. The physical model of the
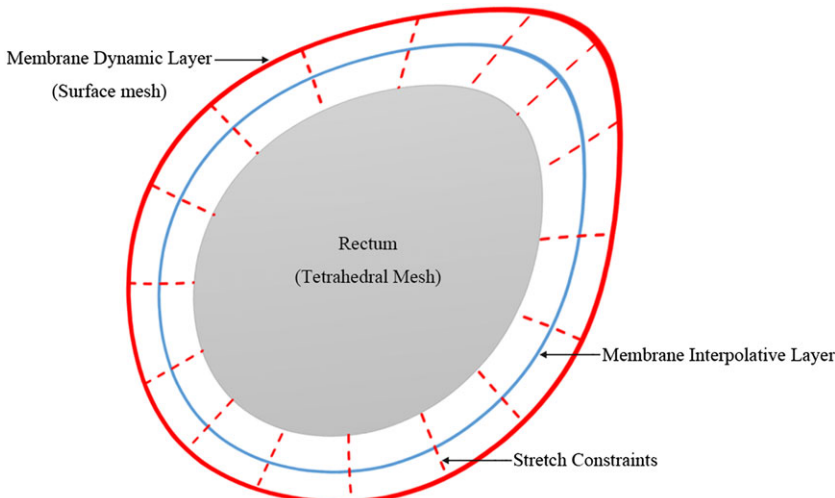

FIGURE 10 Illustration of relationship between rectum, membrane, tetrahedral mesh, surface mesh, dynamic layer, and interpolative layer
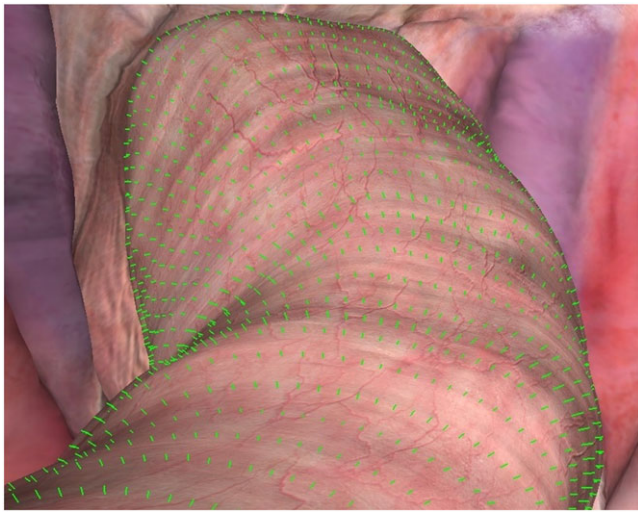
FIGURE 12 Visualization of additional stretch constraints between the membrane and rectum model

abdominal wall supports deformation and movement during surgery simulation.

In the online stage, an explicit forward Euler integration method is employed to compute the velocity and position for each vertex at first. Then external constraints, such as collision and grasping, are detected and generated at the beginning of each time step. We use the geometric method in[18] to detect collisions between surgical tools and surfaces of soft tissue. In the main loop, the solver iteratively updates the position of vertices to satisfy both external and internal constraints. Here, coupled with global springs above, we treat the tetrahedral model and the dynamic layer as one physical system. Finally, the surface mesh of the rectum is updated by barycentric-coordinates mapping.[28] Meanwhile, the position of each node x_i on the interpolation layer can be calculated by linear interpolation between x_p and x_q.

6 | SIMULATION OF ELECTROCAUTERY

The electrocautery uses an adjustable current to heat the soft tissue directly and disconnect the cancerous tissues from the pelvic structure. During the electrocautery procedure of rectal surgery, surgeons have to avoid damaging vulnerable tissues such as the ureter and the nerve plexus. In our work, we start with computation of heat conduction and temperature distribution on the surface of the membrane. Once the tip of the L-hook contacts the surface of the membrane, we fetch the local mapping texture around the contact point to perform the graphic simulation. The temperature distribution $T(\mathbf{x}, t)$ is governed by the two-dimensional bio-heat differential equation[29]:

$$\rho c \frac{\partial T}{\partial t} = k\nabla^2 T + \omega_b c_b (T - T_\alpha) + q_m + q_g, \quad (10)$$

where ∇^2 is the Laplace operator, k is the thermal conductivity of the tissue, ω_b is the effective blood perfusion parameter, c_b is the blood heat capacity, T_α is the blood inlet temperature or steady-state temperature of the tissue, q_m is the metabolic heat generation rate of the tissue, and q_g is the externally generated heat rate from electrosurgical heating. Here we ignore ω_b, c_b and q_m to simplify this equation to

$$\rho c \frac{\partial T}{\partial t} = k\nabla^2 T + q_g, \quad (11)$$

since compared with the external input heat, the energy change caused by metabolism, compression of the tissue and blood flow is so small that it can be ignored. The distributed heat source q_g can be computed by:

$$q_g = J \cdot E, \quad (12)$$

where J is the surface current density (A/m) and E is the electric field intensity (V/m). These two physical quantities can be derived by the Laplace equation[30]:

$$\nabla \cdot (\sigma \nabla V) = 0, \quad (13)$$

where V is the electric potential (V) and σ is the electrical conductivity (S/m). Here we consider the electrical conductivity to be constant for the membrane. The Laplace equation can be solved efficiently and independently. Then we bring the heat source result back to the heat conduction equation. The boundary condition is convective heat loss of the surface. There is:

$$(k\nabla T) \cdot \mathbf{n} + h(T - T_\alpha) = 0, \quad (14)$$

where h is the convection heat transfer coefficient, T_α is the ambient temperature and $\mathbf{n}$ is the unit outward normal on the boundary. Figure 13 shows the temperature distribution when the L-hook tip contacts the membrane. We solve Equation 8 and Equation 10 by the method in.[15]

The visual effects of electrocautery are performed by dynamic temperature texture technology and GLSL rendering. Since we have an extremely high-resolution texture 4096^2 for the rectum model, it is time-consuming and unnecessary to update the whole texture in real time. Using the sub-texture technology and GLSL shader, we can precisely control the rendering effects of electrocautery. Here we extract a 256^2 resolution sub-texture of the original texture of temperature distribution by UV interpolation at each time step. When a collision between the electrosurgical scalpel and the membrane occurs, we search the nearest triangle T and the projection point p of the L-hook tip on T. Then we calculate the barycentric coordinate $(\lambda_1, \lambda_2, \lambda_3)$ of $\mathbf{p}$ in T, where $\mathbf{p} = \lambda_1 \mathbf{p}_1 + \lambda_2 \mathbf{p}_2 + \lambda_3 \mathbf{p}_3$, $\mathbf{p}_1$, $\mathbf{p}_2$, $\mathbf{p}_3$ are three
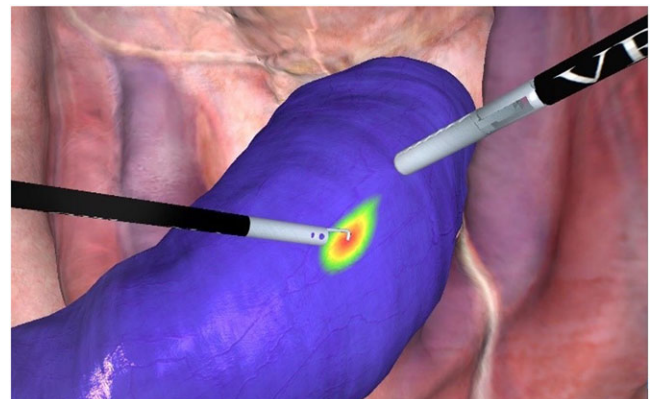

FIGURE 13 Temperature distribution on the surface of membrane model

vertexes of T. The UV coordinate of the sub-texture center is computed by barycentric interpolation. After locating the sub-texture, we update the temperature distribution in this area and transfer to the graphic rendering system.

To show the special biological visual effects of electrocautery, we set two thresholds for different graphic rendering, $v_{vaporization} = 0.988$, and $v_{brown} = 0.95$. We mix the original color with three predefined RGBA colors $C_1 = (1.0, 1.0, 1.0, 0.0)$ $C_1 = (1.0, 1.0, 1.0, 0.0)$, and $C_3 = (0.5, 0.16, 0.16, 0.7)$ referring to the following equation:

$$C_{mix} = \begin{cases} (1-v)C_{ori} + vC_1, v > v_{vaporization} \\ (1-v)C_{ori} + vC_2, v > v_{brown} \\ (1-v)C_{ori} + vC_3, v \leq v_{brown} \end{cases} \quad (15)$$

where $v = \min((T - T_a)(T_{vaporization} - T_a), 1.0)$. The topological modification in electrocautery procedure is based on the change of mass nodes status. We initialize every node in the system with valid status at the beginning. A node turns into invalid status only if its temperature exceeds the threshold of vaporization and it is irreversible. As is shown in Figure 14, once a node becomes invalid, it will affect its surrounding stretch constraints. Supposing P becomes an invalid node, all its connected edges will have a decreased initial length $L_0 = \alpha L_0$, due to the residual strain of the bio-structure. It will pull node P inward with stronger stretches. When node Q becomes invalid, the initial length of four edges will be updated and the edge between P and Q will be deleted.

We compute the haptic feedback when the virtual instrument contacts the membrane tissue or the rectum. It contains a vector of outward normal for the mesh surface and a magnitude, which is proportional to the depth of instrument embedded in the tissue. The parameter coefficient can be set based on biological experiments.

7 | RESULTS

In this section, we present brief qualitative and quantitative results of our implementation in terms of both visual and computational performance. After frequent two-way communications with surgeons and a number of iterative tests, we obtained feasible parameters of PBD (Table 1) and physical properties of tissue (Table 2) in experiments.

During the simulation loop, a shrinking effect of the soft tissue, which benefits from the spring between the rectum and the dynamic
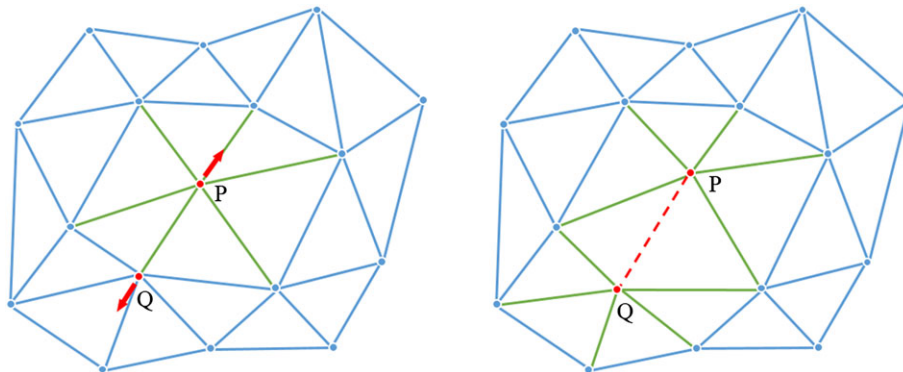
TABLE 1 Values of parameters in our PBD physical system

Parameter	Value
Length of time step (s)	0.2
Number of iterations	3
Stiffness of stretch	0.3
Stiffness of volume	0.9
Stiffness of bending	0.65

TABLE 2 Values of physical properties of tissue in our simulation

Parameter	Value
Thermal conductivity (N/m^2)	0.512
Density (kg/m^3)	3
Specific heat (J/kg K))	0.3
Electrical conductivity (S/m)	0.9

layer of surrounding membrane, will be performed after the drag and release by the grasper. As illustrated in Figure 15 and video, the intestine tissue can deform in real time and give a response to interaction very fast. Figure 16 shows the visual effects of our electrocautery process, which contains texture change, smoking, bleeding and topology modification. Figure 17 illustrates the geometry detail of topology modification on the surface mesh.

We also compare our system with some commercial product. For example, 'LapMentor'(Simibionix), provides a module called 'Sigmoidectomy Procedure', which has soft tissue heat based dissection. Our system has several advantages over their simulator: first, compared with a single PBD model or FEM model, our multi-layer PBD model and dissection method has a plausible performance in simulation of the mechanical behavior of the rectum and the membrane tissue; second, as we can see from the peritoneal incision video of LapMentor, the change of electrocautery incision during the procedure is discontinuous, piece by piece, while our simulation provides a more realistic and continuous visual effect.

8 | COMPUTATIONAL PERFORMANCE

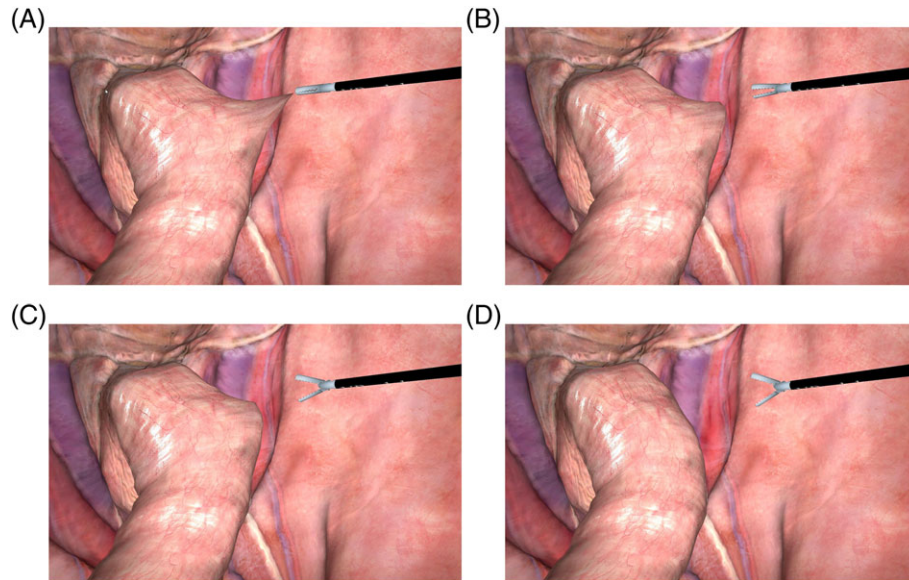The computational performance of our algorithms was tested on a Lenovo desk computer (Win10 X64 Intel Core i7–4790 CPU

FIGURE 14 Topological modification in electrocautery procedure. All stretch constraints connected with the node P (green lines) are modified to shrink because of the residual strain (*left*). If node Q becomes invalid, both P and Q will separate away from each other and PQ is deleted (*right*)

FIGURE 15　Deformation of the rectum, which is dragged and released by a grasper, 15 A, 0 ms, 15 B, 30 ms, 15 C, 100 ms, 15 D, 1000 ms
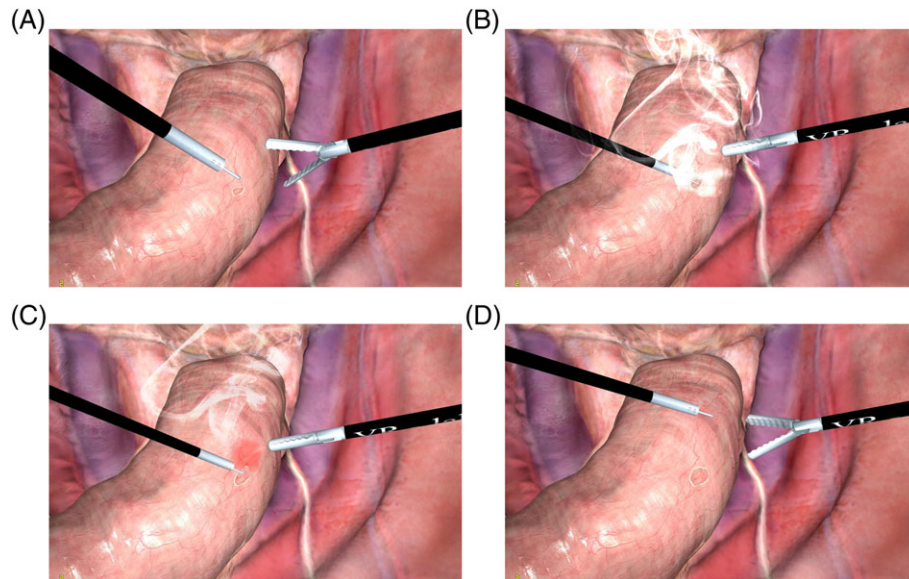

FIGURE 16　Screenshots of cautery procedure on the membrane: A, before cautery; B, smoking effect during cautery; C, bleeding effect during cautery; D, after cautery

3.60GHz, 8GB RAM, NVIDIA GeForce GTX 760). The haptic refreshing frequency was >1000 Hz and the graphic display was updated at a standard 60 frames per s. Here we present a pie chart of computation cost percentage for all tasks in simulation (Figure 18). We also compare our techniques with the work in Pan et al.,[18] which used a mass–spring system to simulate the behavior of the rectum in LP surgery. Table 3 gives comparison results. Our simulation has a significant improvement in the following aspects:

1. computation performance: our implementation reached a 105 FPS versus 45 FPS in previous work;

2. complexity of model: we built a larger scale scene with detailed geometric information and texture;

3. physical accuracy: volume conservation can be expressed by multiple types of PBD constraints in our implementation.

Our PBD system has a very similar complexity with Qian et al.[17] topology-unchanged projective dynamics system (see Table 4), because both of them meet the same minimization problem and do not add new vertices into the system. We have a more accurate physics-based energized model, which is governed by a bio-heat differential equation, while Qian et al. assumed that there is no heat transfer on the soft tissue. Since a customized texture mapping rendering technique is applied, our method can provide a more realistic and continuous visual result, especially when the mesh has a relatively low resolution.

9 | VALIDATION

We invited 15 surgeons from the general surgery department of The Affiliated Hospital of Qingdao University to test and evaluate our
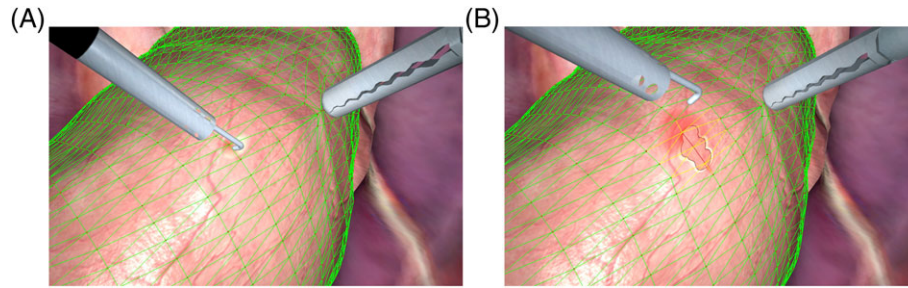
FIGURE 17   Stretch constraints before cautery (*left*) and topology modification after cautery (*right*). Constraints in red were deleted, constraints in yellow were modified by $L_0 = 0.7L_0$
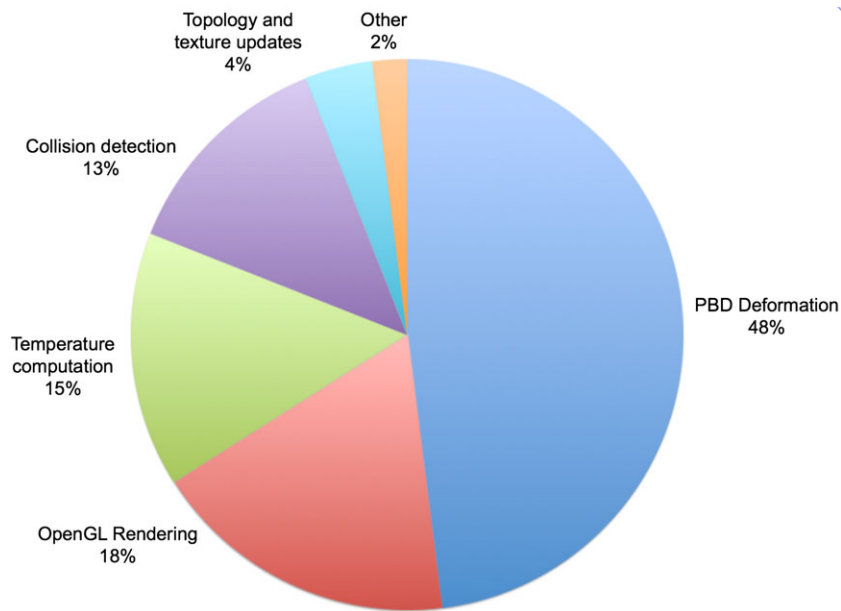

FIGURE 18   Distribution of computation cost for all tasks in one simulation time step. The most time-consuming task is PBD deformation, which takes 4.71 ms

TABLE 3   Comparison of model complexity and computational performance in respect to the work of pan *et al.*[18]

	Pan *et al.*	Ours
Number of vertexes	4743	20556
Number of stretch constraints	17982	65279
Number of volume constraints	0	6105
Number of bending constraints	0	1853
Time per time step (ms)	22.34	9.48
Frames per second	44.76	105.49

TABLE 4   Comparison of model complexity and computational speed in respect to the work of Qian *et al.*[17]

	Qian K *et al.*	Ours
Number of tetrahedrons	30 K	6 K
Frames per second	15.1	105.5

system. A verification of clinical realism and the effectiveness of training was carried out by a pilot study. We collected subjective feedback through a questionnaire consisting of 12 questions:

(1) realism of the anatomy; (2) realism of the appearance of the simulator interface; (3) realism of the instrument handling; (4) realism of the electrocautery task; (5) realism of deformation during traction; (6) realism of eye–hand coordination system; (7) realism of training compared with traditional laparoscopic operation; (8) quality and realism of force feedback; (9) usefulness in learning haptic experiences and skills; (10) usefulness in learning hand–eye coordination; (11) usefulness in learning ambidexterity skills; (12) overall usefulness in learning the fundamental surgical skills. All these questions were answered on a scale of 1 to 5, with 0 for very poor and 5 for very good. Table 5 shows the results of this questionnaire.

Our simulation showed good overall realism and usefulness. In the questionnaire, 93% of participants consider the deformation of soft tissues were realistic (i.e. 4 or 5) and 86% of participants regarded realism

TABLE 5   Statistics of the questionnaire

	1	2	3	4	5	6	7	8	9	10	11	12
Mean	3.9	4.3	3.9	4.3	4.6	3.4	3.8	3.6	3.8	4.2	4.0	3.9
SD	0.61	0.65	0.76	0.53	0.26	1.08	0.53	0.73	0.96	0.45	0.52	1.18

of the appearance of the simulator interface was good. For the electrocautery task, 80% of responses were 4 or more, indicating a plausible visual realism. Overall usefulness in learning fundamental surgical skills got a 3.9 average score among all responses, which means that majority of the participants agreed good usefulness in training of LS skills.

10 | CONCLUSION

In this paper, we have presented a well-developed VR simulator for laparoscopic radical cancer surgery. It is equipped with a new designed surgery instrument handle. The continuous state collection makes the virtual instrument, such as grasper, precisely controlled. In the software development, we focus on promoting the efficiency and the physical accuracy of soft tissue deformation. Here we employ a PBD framework, which can impose various physics-based constraints such as stretch, volume conservation and bending, allowing realistic deformation in a robust and efficient way. A multi-layer PBD model has been designed to better describe the mechanical behavior of the rectum and its surrounding membrane tissues. Both the experimental data and the subjective feedback from surgeons have proved that our system can realistically simulate the deformable rectum and membrane in real time. A bio-heat conduction based temperature computation model has also been proposed to simulate the electrocautery procedure, guaranteeing a physical basis for topology update and texture manipulation on the membrane surface.

These initial results and validation infer that our simulator provides a physics-based interactive platform for basic skill training of laparoscopic radical cancer surgery. The realistic deformation of soft tissue can be similarly implemented for a wide range of human organs, in other advanced laparoscopic procedures.

11 | LIMITATIONS AND FUTURE WORK

A major limitation of our simulation system is that the interaction of electrocautery only occurs on the surface of the membrane. In a next step, a volume-based method for topology update and rendering is required to fix this defect. In a preliminary validation study, our system has shown its overall realism and usefulness in surgical training, however, there is a lack of some noticeable cues in our scenario, such as the ureter and the nerve plexus. Instructions and warnings should be given when a trainer burns these wrong areas by mistake. We will also consider a more complex haptic algorithm and device, i.e. the Phantom Premium, which can provide multi-point haptic feedback.

Among the results in the questionnaire, the lowest scores are for 'quality and realism of force feedback' (Table 4). We are considering some more advanced algorithms of tactile and haptic feedback[31] to replace the basic method provided by OpenHaptics API. As the position-based projective methods have been further developed in recent years,[32-35] our traditional PBD framework for the soft body model is relatively simple. It would be necessary to investigate more effective numerical methods and GPU parallel solver to handle complicated physical simulation in surgery.

CONFLICT OF INTEREST STATEMENT

We declare that we have no financial and personal relationships with other people or organizations that can inappropriately influence our work, there is no professional or other personal interest of any nature or kind in any product, service and/or company that could be construed as influencing the position presented in, or the review of, the manuscript entitled.

REFERENCES

1. Veldkamp R, Kuhry E, Hop WC, et al. Laparoscopic surgery versus surgery for colon cancer: Short-term outcomes of a randomised trial. *Lancet Oncol*. 2005;6(7):477-484.

2. SEER cancer statistics from USA National Institutes of health. https://seer.cancer.gov/statfacts/html/colorect.html

3. http://colorectalsurgeonssydney.com.au/?page_id=418/

4. Bonjer HJ, Haglind E, Cuesta MA, et al. Laparoscopic surgery versus open surgery for rectal cancer: Short-term outcomes of a randomised trial. *Europ J Cancer*. 2011;47(11):4-4.

5. Akdemir A, Zeybek B, Ergenoglu AM, Yeniel AO, Sendag F. Effect of spaced training with a box trainer on the acquisition and retention of basic laparoscopic skills. *Int J Gynaecol Obstet Official Organ Int Fed Gynaecol Obstet*. 2014;127(3):309-313.

6. International Agency for Research on Cancer. Colorectal cancer estimated incidence, mortality and prevalence worldwide in 2012. http://globocan.iarc.fr/Pages/fact_sheets_cancer.aspx/

7. Korzeniowski P, Barrow A, Sodergren MH, Hald N, Bello F. NOViSE a virtual natural orifice transluminal endoscopic surgery simulator. *Int J Comput Assist Radiol Surg*. 2016;1-13.

8. Pan JJ, Chang J, Yang X, et al. Graphic and haptic simulation system for virtual laparoscopic rectum surgery. *Int J Med Robot Comput Assist Surg*. 2011;7(3):304-317.

9. Yuan ZY, Ding YH, Zhang YY, Zhao JH. Real-time simulation of tissue cutting with CUDA based on GPGPU. *Adv Mater Res*. 2010;121–122:154-161.

10. Muller M, Stam J, James D, Rey N. Real time physics: Class notes. *ACM SIGGRAPH*. 2008;1-90.

11. Muller M, Dorsey J, Mcmillan L, Jagnow R, Cutler B. Stable real-time deformations. ACM International Conference on Computer Graphics and Interactive Techniques, 2002; 49–54.

12. Irgens F. *Continuum Mechanics*. Berlin, Heidelberg: Springer; 2008.

13. Dodde RE, Miller SF, Shih AJ, Geiger JD. Thermal-electric finite element analysis of electrosurgical cautery process. *ASME International Manufacturing Science and Engineering Conference*. 2007;665-671.

14. Maciel A, De S. Physics-based real time laparoscopic electrosurgery simulation. *Studies Health Technol Informat*. 2008;132(1):272-274.

15. Lu Z, Arikatla VS, Han Z, Allen BF, De S. A physics-based algorithm for real-time simulation of electrosurgery procedures in minimally invasive surgery. *Int J Med Robot Comput Assist Surg*. 2014;10(4):495-504.

16. Wu J, Westermann R, Dick C. Real-time haptic cutting of high-resolution soft tissues. *Studies Health Technol Informat*. 2014;196:469-475.

17. Qian K, Jiang T, Wang M, Yang X, Zhang J. Energized soft tissue dissection in surgery simulation. *Comput Animat Virtual Worlds*. 2016;27(3–4):280-289.

18. Pan JJ, Chang J, Yang X, et al. Virtual reality training and assessment in laparoscopic rectum surgery. *Int J Med Robot Comput Assist Surg*. 2014;11(2):194-209.

19. Nealen A, Muller M, Keiser R, Boxerman E, Carlson M. Physically based deformable models in computer graphics. *Comput Graphics Forum*. 2006;25(4):809-836.

20. Goemagic touch (formerly Sensable phantom Omni). http://www.geomagic.com/en/products/phantom-omni/overview/

21. Zienkiewicz OC, Taylor RL, Zhu JZ. *The Finite Element Method: Its Basis and Fundamentals*. Butterworth-Heinemann; 2005.

22. Xu H, Barbic J. Pose-space subspace dynamics. *Acm Trans Graphics*. 2016;35(4):35

23. Liu T, Bouaziz S, Kavan L. Towards real-time simulation of hyperelastic materials. Technical Report 1604.07378 (2016).

24. Muller M, Heidelberger B, Hennix M, Ratcliff J. Position based dynamics. *J Visual Commun Image Represent*. 2007;18(2):109-118.

25. Mafalda C, Erik M, Ara D, Pratt P. Soft tissue deformation for surgical simulation: A position-based dynamics approach. *Int J Comput Assist Radiol Surg*. 2016;11(6):1-10.

26. Pan J, Bai J, Zhao X, Hao A, Qin H. Real-time haptic manipulation and cutting of hybrid soft tissue models by extended position-based dynamics. *Comput Animat Virtual Worlds*. 2015;26(3–4):321-335.

27. Skala V. Barycentric coordinates computation in homogeneous coordinates. *Comput Graphics*. 2008;32(1):120-127.

28. Bender J, Muller M, Otaduy MA, et al. A survey on position-based simulation methods in computer graphics. *Comput Graphics Forum*. 2014;33(6):228-251.

29. Pennes HH. Analysis of tissue and arterial blood temperatures in the resting human forearm. *J Appl Physiol*. 1998;85(1):5-34.

30. Berjano EJ. Theoretical modeling for radiofrequency ablation: State-of-the-art and challenges for the future. *Biomed Eng Online*. 2006;5(1):24

31. Wang D, Liu S, Zhang X, Zhang Y. Six-degree-of-freedom haptic simulation of organ deformation in dental operations. *Int Conf Robot Autom*. 2012:1050-1056.

32. Macklin M, Muller M, Chentanez N. XPBD: Position-based simulation of compliant constrained dynamics. *Motion in Games*. 2016:49-54

33. Bouaziz S, Martin S, Liu T, Kavan L, Pauly M. Projective dynamics: Fusing constraint projections for fast simulation. *ACM Trans Graphics*. 2014;33(4):70-79.

34. Wang H. A chebyshev semi-iterative approach for accelerating projective and position-based dynamics. *ACM Trans Graphics*. 2015;34(6):1-9.

35. Wang H, Yang Y. Descent methods for elastic body simulation on the GPU. *ACM Trans Graphics*. 2016;35(6):1-10.

SUPPORTING INFORMATION

Additional Supporting Information may be found online in the supporting information tab for this article.

APPENDIX A

A.1 | Final positional corrections of stretch constraint

$$\Delta\mathbf{p}_1 = -\frac{w_1}{w_1+w_2}(|\mathbf{p}_1-\mathbf{p}_2|-d)\frac{\mathbf{p}_1-\mathbf{p}_2}{|\mathbf{p}_1-\mathbf{p}_2|} \qquad (A1)$$

$$\Delta\mathbf{p}_2 = +\frac{w_2}{w_1+w_2}(|\mathbf{p}_1-\mathbf{p}_2|-d)\frac{\mathbf{p}_1-\mathbf{p}_2}{|\mathbf{p}_1-\mathbf{p}_2|} \qquad (A2)$$

A.2 | Final positional corrections of volume conservation constraint

$$\Delta\mathbf{p}_i = -w_i\mathbf{q}_i(V-V_0)/\sum_j\left(w_j|\mathbf{q}_j|^2\right) \qquad (A3)$$

A.3 | Final positional corrections of bending constraint

$$\Delta\mathbf{p}_i = -\frac{4w_i}{\sum_j w_j}\frac{\sqrt{1-d^2}(\arccos(d)-\varphi_0)}{\sum_j|\mathbf{q}_j|^2}\mathbf{q}_i \qquad (A4)$$

where

$$d = \frac{(\mathbf{p}_2-\mathbf{p}_1)\times(\mathbf{p}_3-\mathbf{p}_1)}{|(\mathbf{p}_2-\mathbf{p}_1)\times(\mathbf{p}_3-\mathbf{p}_1)|}\cdot\frac{(\mathbf{p}_2-\mathbf{p}_1)\times(\mathbf{p}_4-\mathbf{p}_1)}{|(\mathbf{p}_2-\mathbf{p}_1)\times(\mathbf{p}_4-\mathbf{p}_1)|} \qquad (A5)$$